NANO LETTERS

Letter

pubs.acs.org/NanoLett

Tunable Phonon-Induced Transparency in Bilayer Graphene Nanoribbons

Hugen Yan,*[,†,⊥] Tony Low,*[,†,⊥] Francisco Guinea,[‡] Fengnian Xia,*[,†,§] and Phaedon Avouris*[,†]

[†]IBM Thomas J. Watson Research Center, Yorktown Heights, New York 10598, United States

[‡]Instituto de Ciencia de Materiales de Madrid (CSIC), Sor Juana Inés de la Cruz 3, 28049 Madrid, Spain

[§]Department of Electrial Engineering, Yale University, New Haven, Connecticut 06511, United States

Supporting Information

ABSTRACT: In the phenomenon of plasmon-induced transparency, which is a classical analogue of electromagnetically induced transparency (EIT) in atomic gases, the coherent interference between two plasmon modes results in an optical transparency window in a broad absorption spectrum. With the requirement of contrasting lifetimes, typically one of the plasmon modes involved is a dark mode that has limited coupling to the electromagnetic radiation and possesses relatively longer lifetime. Plasmon-induced transparency not only leads to light transmission at otherwise opaque frequency regions but also results in the slowing of light group velocity and enhanced optical nonlinearity. In this article, we report an analogous behavior, denoted as phonon-induced transparency (PIT), in AB-stacked bilayer graphene nanoribbons. Here, light absorption due to the plasmon excitation is suppressed in a narrow window due to the coupling with the infrared active Γ-point optical phonon, whose function here is similar to that of the dark plasmon mode in the plasmon-induced transparency. We further show that PIT in bilayer graphene is actively tunable by electrostatic gating and estimate a maximum slow light factor of around 500 at the phonon frequency of 1580 cm^{-1}, based on the measured spectra. Our demonstration opens an avenue for the exploration of few-photon nonlinear optics and slow light in this novel two-dimensional material.

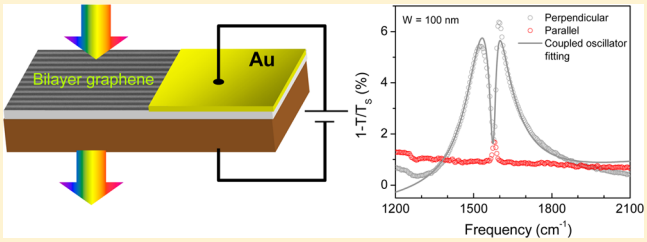

KEYWORDS: *graphene, phonon-induced transparency, plasmon, slow light*

Since the early demonstration of electromagnetically induced transparency (EIT) in atomic gases,[1] analogous physical situations have been implemented in various solid state systems. This includes coupled optical resonators,[2] metallic plasmonic structures,[3−6] and optomechanical systems.[7] A plasmonic analogue of EIT utilizes the destructive interference effect between a radiative and a dark plasmon mode of different lifetimes.[3] A major motivation for the exploration of the EIT-like phenomenon in solid state systems is its potential in integrated photonic systems[2,8] for computing, optical communications, and biosensing[9] made possible by the enhanced light group index and nonlinearity within the spectral transparency window.

Graphene, with its unique relativistic-like linear energy dispersion, has emerged as a promising platform for plasmonics[10−14] due to its electrical tunability, strong light confinement, and relatively low plasmonic losses.[14] Very recently, spatially resolved propagating plasmons and tunable localized plasmons have been observed over a broad range of frequencies from the terahertz to the mid-infrared.[10−13] Besides graphene, several allotropes of carbon can also exhibit the above-mentioned attractive attributes for plasmonics. In this work, we focus on plasmons in bilayer graphene, showing that it is both an interesting and important plasmonic material in its own right.

The optical conductivity of AB-stacked bilayer graphene exhibits several interesting infrared features as revealed in recent measurements.[15−17] In particular, the coupling between the two graphene layers in bilayer graphene induces infrared activity on its Γ-point optical phonon, which exhibits a Fano-type[18] resonance in its infrared optical conductivity under certain circumstances.[16,17] The Fano resonance is related to the presence of discrete states (i.e., phonon in this case) interacting coherently with a single particle continuum (electronic transitions). With the excitation of a different kind of quasiparticle, plasmon, we demonstrate a phonon−plasmon Fano resonance system due to coherent interactions between the long-lived lattice vibration mode and the quasicontinuum plasmon mode of bilayer graphene nanoribbons. An extremely narrow transparency window in the spectral response is observed, centered near the phonon frequency, when the plasmon frequency coincides with the phonon frequency. To distinguish this from the widely studied plasmon-induced transparency,[3−6,9] which typically involves two plasmon modes, we call the newly observed effect the "phonon-induced

Received: May 1, 2014
Revised: July 3, 2014
Published: July 14, 2014

transparency" (PIT), a term that has been occasionally used in the literature under different circumstances.[19] This new effect modifies the infrared plasmonic response of bilayer graphene in drastic ways. At the spectral transparency, it is expected to be accompanied by sharp increase of the group index (or decrease of group velocity) and enhancement of the optical nonlinearity. A very wide degree of PIT tunability, both active and passive, is also demonstrated through electrostatic gating, chemical doping, and ribbon width control. Our experimental results are found to be in good agreement with theoretical calculations, performed on a microscopic quantum mechanical footing. The PIT demonstrated in the current paper is another classical analogue of EIT, with the phonon mode corresponding to the metastable state in the three-level atomic system in conventional EIT. Moreover, the plasmon−phonon coupling corresponds to the pump laser which couples the metastable state and the dipole allowed excited state.[1]

The measurement scheme used in this study is shown in Figure 1a. Large AB-stacked bilayer graphene flakes (>100 μm in size) were exfoliated from graphite through mechanical cleavage and identified by Raman spectroscopy[20] (Supporting Information). The extinction spectra were obtained by comparing the transmission through the substrate with patterned bilayer graphene ribbons (or unpatterned bilayer graphene) and the bare substrate. Detailed sample preparation and characterization methods are presented in Methods. Figure 1b shows an infrared extinction spectrum ($1 - T/T_S$) of an unpatterned bilayer graphene. In this case, the transmission T is independent of the light polarization. The first prominent feature in Figure 1b is the broad extinction peak around 3500 cm^{-1}, which originates from the low energy electronic transitions,[15] as shown in the lower inset. The second feature is the sharp phonon absorption peak at around 1580 cm^{-1}. The full width at half-maximum (fwhm) of the peak is about 10 cm^{-1}. Previous studies have shown that the absorption magnitude and line-shape of the phonon depend strongly on the Fermi level and electrical field across the two graphene layers,[16,17] which can be described by the charged phonon theory.[21,22] For the samples we studied here, the phonon line shape does not show strong asymmetry if plasmons are not excited.

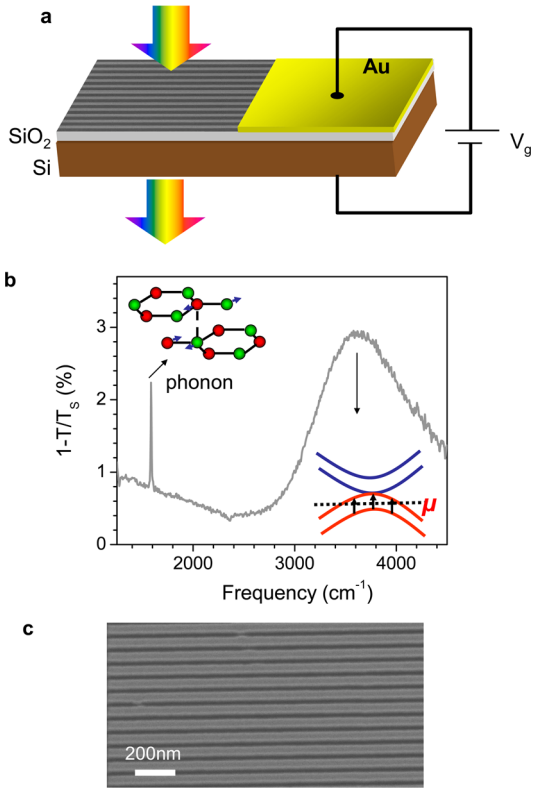

Figure 1. Schematics of the experiment. (a) Extinction spectrum measurement scheme for a gate-tunable bilayer graphene nanoribbon array for parallel and perpendicular light polarization. (b) Extinction spectrum of an unpatterned bilayer graphene flake. The lower right inset depicts the low energy band structure of bilayer graphene with hole-doping (μ < 0) and the dominant electronic transition responsible for the absorption peak is indicated. Upper left inset shows the lattice vibration responsible for the phonon absorption. (c) Scanning electron micrograph of a typical graphene nanoribbon (90 nm ribbon width) array used in the experiment. The scale bar is 200 nm.

We patterned large area bilayer graphene into nanoribbons using electron beam lithography and reactive-ion etching (see Methods). In this manner, plasmons can be excited using normal light incidence. Figure 1c shows a scanning electron micrograph (SEM) of a typical bilayer graphene nanoribbon array (ribbon width ∼ 90 nm). The extinction spectra of an array with a ribbon width of 130 nm are shown in Figure 2a, for light polarizations both perpendicular and parallel to ribbons. These two spectra are dramatically different due to the excitation of localized plasmon in the perpendicular polarization case,[14] in which two prominent plasmon resonance peaks at around 1000 and 1400 cm^{-1} are observed. These are coupled modes of plasmon and the surface polar phonon of the underlying SiO_2 substrate.[14,23] With an arbitrary light polarization, the spectrum is a linear superposition of the two spectra with perpendicular and parallel polarizations. Throughout this work, we focus on the higher frequency plasmon mode (the one centered at ∼1400 cm^{-1} in Figure 2a). Moreover, a strong graphene phonon peak with an extinction of >5% exists at 1580 cm^{-1}. The extracted phonon peak as shown in the inset has a typical Fano line-shape,[18] a result of interference between the sharp phonon resonance and the broad plasmon peak. The same phonon peak is also observed when the incident light polarization is parallel to the ribbons (gray curve) with much smaller extinction (<2%) and nearly symmetric line shape. This large difference in the magnitude of the phonon extinction indicates that the coupling of external light to the phonon mode is enhanced significantly through plasmon excitation. This is analogous to that in plasmon-induced transparency, in which coupling of the external light excitation to the dark mode is enhanced through the radiative mode.[3] The phonon spectrum peak frequency also shifts slightly (∼6 cm^{-1}) when we change the light polarization due to the Fano resonance effect which pushes the phonon spectrum peak to a higher frequency in the perpendicular polarization case.

Decreasing ribbon width leads to an increase in the plasmon wave vector, resulting in an enhancement in plasmon resonance frequency, as previously demonstrated.[14] Figure 2b displays the extinction spectra of a ribbon array with width of 100 nm. When the plasmon frequency approaches the phonon frequency, the extinction spectrum exhibits a narrow transparency window at the phonon frequency, in sharp contrast to the case of light excitation with parallel polarization, in which an absorption peak shows up. This transparency window is due to the destructive interference of two optical transition

dx.doi.org/10.1021/nl501628x | Nano Lett. 2014, 14, 4581−4586

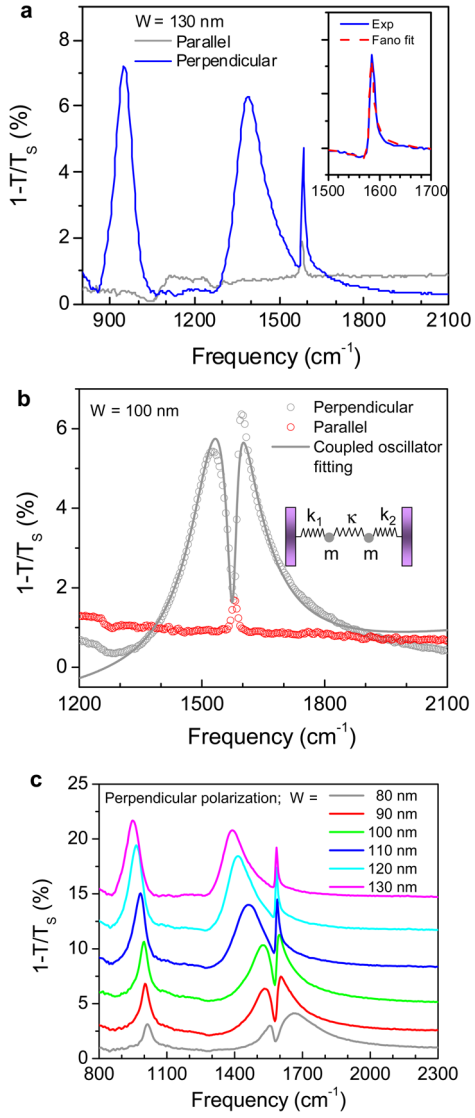

Figure 2. Plasmon–phonon Fano system and phonon-induced transparency in bilayer graphene nanoribbons. (a) Extinction spectra of a ribbon array with W = 130 nm for two incident light polarizations: parallel and perpendicular to the ribbons. The inset shows the extracted phonon spectrum with a Fano fit for perpendicular polarization case. (b) Extinction spectra of a ribbon array with W = 100 nm. The spectrum for the perpendicular polarization is fitted by the coupled oscillator model, as shown by the solid curve. The inset depicts the coupled oscillator model scheme which is discussed in detail in the Supporting Information. (c) Ribbon width dependence of the spectra for the coupled plasmon–phonon Fano resonance system. Spectra are shifted vertically for clarity.

pathways: excitations of a plasmon mode and a phonon mode. Compared to the typical plasmon-induced transparency where destructive interference of two plasmon modes are utilized, the PIT in bilayer graphene here has sharper transparency window due to the long phonon lifetime. The phonon lifetime is at least 1 order of magnitude larger than that of the plasmon mode in graphene and other plasmonic materials. This is desirable for applications such as slow light[24] and low-light level optical nonlinearity.[25] In conventional plasmon-induced transparency, the dark plasmon mode, although longer lived than that of the radiative (bright) mode, still has very limited quality factor (a quality factor only about 2–4 times larger than that of the bright mode[5]). Although utilization of superconductors as the plasmonic material can increase the dark mode's lifetime, because carrier scattering is suppressed in its superconducting state, it requires liquid helium temperature.[6] In this regard, bilayer graphene is a naturally superior material for this purpose, operating at room temperature.

We use a phenomenological theory involving two coupled classical oscillators[26] (as shown in the inset of Figure 2b) to describe the PIT and the Fano resonance of the phonon feature. The details of the model are presented in the Supporting Information. The solid line in Figure 2b shows the fitted response, using a coupling strength of ~300 cm^{-1} between the plasmon mode and the phonon mode. The microscopic origin of the coupling strength is from the electron–phonon interaction in the bilayer graphene system and will be discussed later in the paper. In this model, if the coupling strength is too large, the resulting extinction spectrum constitutes two well-separated modes, and no narrow transparency window can be observed. For example, the hybridization of the graphene plasmon with SiO_2 surface polar phonon modes results in multiple, well-separated extinction peaks[14] (see spectra in Figure 2a and c). On the other hand, if the plasmon–phonon coupling is too weak, the dip in the extinction spectrum will be small and such a small perturbation will not affect the group velocity and nonlinear properties significantly (Supporting Information). This is usually the case for the plasmon coupling to the molecular vibrations of attached molecules.[27] The coupling of plasmon to the infrared active phonon mode in bilayer graphene has the optimal strength such that a pronounced PIT effect can be observed. On the contrary, for thicker graphene sheets with three or four layers, we observe a less pronounced PIT effect. This is probably due to the weaker plasmon–phonon coupling in those multilayer systems (see Supporting Information). More studies are needed for multilayer graphene, given the fact that the phonon behavior and electron–phonon coupling have strong dependence on the stacking order of the graphene layers.[28] Although for single layer graphene, PIT originated from the intrinsic phonon of graphene does not exist due to the infrared inactivity of the phonons. However, the plasmon can couple to extrinsic molecular vibrations[29] or lattice vibrations[30] to exhibit EIT-like phenomena. It should be emphasized that the EIT-like effect is typically accompanied by Fano resonances. However, not every Fano resonance effect can achieve EIT-like phenomenon due to the more stringent conditions, such as a proper coupling strength between two modes, large line width contrast, and coincidence of their resonance frequencies. Bilayer graphene plasmonic metamaterials can satisfy all these requirements.

In addition to the optimal plasmon–phonon coupling, the PIT and the phonon–plasmon Fano resonance system in bilayer graphene are tunable. Figure 2c displays the extinction spectra for ribbon arrays with widths varying from 130 to 80 nm. The higher frequency plasmon peak can be tuned from below to above the phonon frequency. Figure 2c clearly demonstrates the evolution process of the phonon line-shape, which varies from an enhanced Fano peak (130 nm ribbon) to a PIT-like absorption dip (100 nm ribbon) and finally a Fano peak again (80 nm ribbon).

Furthermore, the PIT can be tuned by doping as well. Figure 3a indicates the spectra for a ribbon array (100 nm) at different levels of chemical doping. The doping control procedure is detailed in the Methods. With this method, we have no direct

dx.doi.org/10.1021/nl501628x | Nano Lett. 2014, 14, 4581–4586

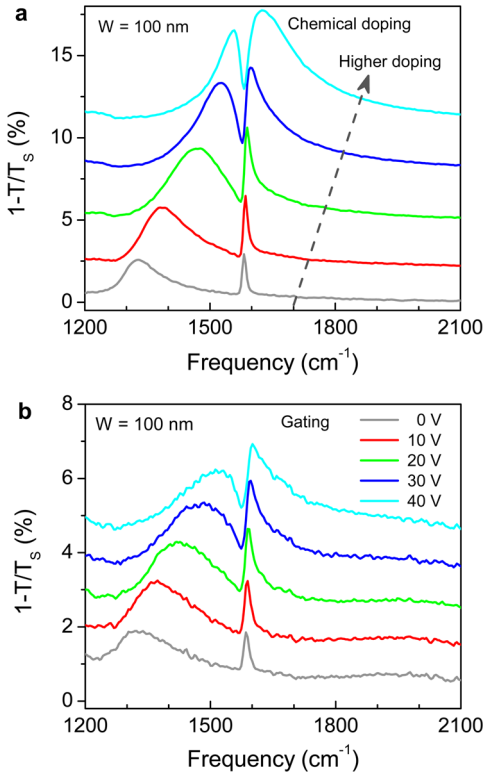

Figure 3. Tunable phonon-induced transparency. (a) Extinction spectrum evolution with increasing chemical doping for a ribbon array with W = 100 nm for perpendicular polarization. (b) Spectrum evolution with increasing back-gate voltage for a gated nanoribbon array device. Spectra are shifted vertically for clarity.

quantitative evaluation of the doping concentration in bilayer graphene, though indirect information based on the single layer graphene on the same wafer is available through the Pauli blocking phenomenon in the mid-IR spectrum.[31,32] The Fermi energy roughly increases from −0.3 to −0.4 eV. With increasing doping, the plasmon frequency up-shifts from below to above the phonon frequency. The extinction spectra evolve in a manner similar to that in Figure 2c. Most importantly, the PIT in bilayer graphene can be actively controlled using electrostatic gating. Active control of conventional plasmon-induced transparency has been demonstrated recently through ultrafast laser excitations[4] and through temperature tuning of the superconducting elements.[6] We fabricated metal contacts on ribbons and gated the ribbons using a silicon back gate (see Methods), as illustrated in Figure 1a. Figure 3b presents the extinction spectra of a ribbon array (100 nm) with different back gate voltages. Again, PIT tunability is demonstrated. Here, we want to emphasize that the group indices and nonlinear properties associated with PIT are at the same time also tunable using gating, which may have significant impact on the future exploration of this bilayer graphene phonon-plasmon system. A key parameter which describes the Fano line-shape of the phonon feature depends solely on the detuning of the plasmon frequency from that of the phonon. An analysis of the dependence is detailed in the Supporting Information.

We have experimentally demonstrated a unique plasmonic system with bilayer graphene, where the interference between the plasmon and phonon modes leads to widely tunable Fano effect and PIT. Below, we present simulation results performed on a microscopic quantum mechanical level on this novel effect that allow new insights into the phenomenon. This complements the phenomenological model used earlier in the paper and provides microscopic description of the phonon−plasmon coupling. We consider a bilayer graphene arranged in the Bernal AB stacking order as depicted in the inset of Figure 1b. Following McCann,[33] we work in the 4 × 4 basis of atomic p_z orbitals (see Methods). The central quantity of interest is the dynamic dielectric function of the system $\varepsilon_T^{RPA}(q, \omega)$, which is calculated from the random phase approximation (RPA). The coupling of the two optical in-plane phonons at Γ-point (i.e., the symmetric E_g and the antisymmetric E_u modes) with the optically allowed electronic particle-hole transitions follows a formalism known as the charged-phonon theory,[21,22] which accounts for the strong coupling between phonons and electronic transitions in an otherwise nonpolar system like graphene. We defer further descriptions to the Supporting Information.

The experimentally measured plasmon extinction spectrum is related to the RPA loss function $L(q, \omega) \equiv -\mathrm{Im}\,[1/\varepsilon_T^{RPA}]$.[34−36] In this work, we use the simple mapping between plasmon momentum and the ribbon's width $q = \pi/(W - W_0)$, where W_0 denotes the width of the electrically dead zone.[14] Figure 4a shows the calculated RPA loss spectra for bilayer graphene assuming the case for zero gap, that is, Δ = 0 eV. In order to make comparison with experimentally measured extinction spectra, we employ in our simulations parameters accounting

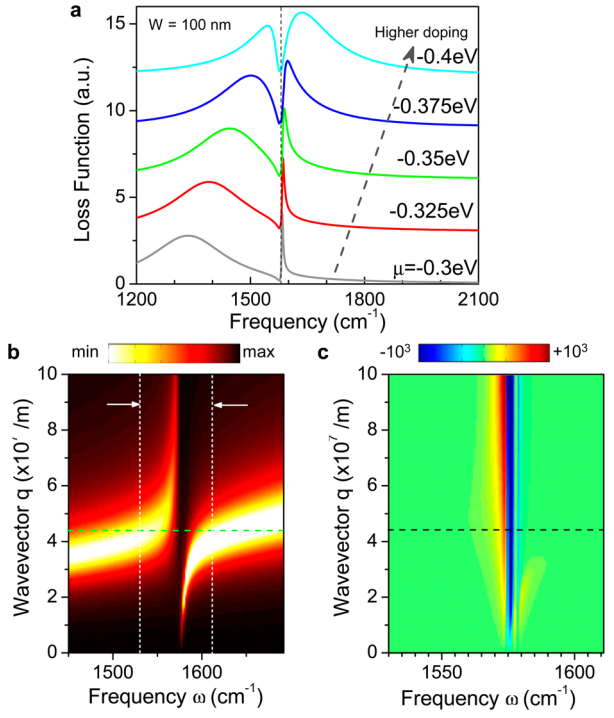

Figure 4. Theoretical simulations of phonon-induced transparency and slow light. (a) Loss function, $L(q,\omega)$, of bilayer graphene simulated at particular $q = q_0$ corresponding to W = 100 nm. The different spectra (shifted vertically for clarity) are calculated at different Fermi level ranging from −0.3 to −0.4 eV. See text for detailed simulation parameters. 2-dimensional intensity plots of $L(q,\omega)$ and group index $n_g(q,\omega)$ for the highest doping case, that is, μ = −0.4 eV, are shown in b and c. The value of q_0 is also indicated by the horizontal lines. Vertical dashed lines in panel b indicate the corresponding plot area of panel c.

dx.doi.org/10.1021/nl501628x | Nano Lett. 2014, 14, 4581−4586

for known experimental conditions and knowledge acquired from prior work[14]

$$q = \pi/(W - W_0) = 4.4 \times 10^7\ \mathrm{m}^{-1}$$

which correspond to ribbon array with W = 100 nm, W_0 = 28 nm, T = 300 K, ε_{env} = 1.5, phonon lifetime of 10 ps and doping ranging from $\mu \approx -0.3 \rightarrow -0.4$ eV which is in agreement with our experimental doping conditions. Finite electronic lifetimes is accounted for through the substitution $\hbar\omega \rightarrow \hbar\omega + i\eta$, where we assumed typical value of $\eta \approx 10$ meV.The qualitative agreement between our experimentally observed extinction spectra in Figure 3a and the simulated result is satisfactory. In particular, the model describes well the evolution of the plasmon and infrared phonon resonances as they approach each other; going from separate resonances to the Fano-like asymmetric spectral line-shapes, and eventually an induced sharp transparency when their resonant frequencies coincide.

Figure 4b shows an intensity plot of the loss function $L(q,\omega)$in the vicinity of the phonon resonant frequency at 1580 cm^{-1}. With close to zero detuning, contrasting resonance line widths and appropriate coupling strength between the two modes, destructive interference suppresses the absorption of the broader resonance, resulting in a very narrow transparency window. Figure 4b also shows a large transfer of spectral weight to the infrared phonon with decreased detuning, as reflected by the increase in both intensity and line width. The new elementary excitation leads to a "dressed" phonon with more pronounced infrared activity renormalized by electron−phonon interactions. Comparison between the spectral weight of phonon mode with and without plasmon hybridization indicates a 100-fold enhancement in infrared activity, consistent also with experimental observation (see Figure 2a).

EIT is also known for its drastic modifications to the medium dispersion characteristics.[24] Recall that the group velocity describing propagation of wave packets can be expressed as $v_g = c/n_g$, where the group index is defined as $n_g \equiv n_r + \omega \cdot dn_r/d\omega$, with $n_r = \mathrm{Re}[(\varepsilon_T^{RPA})^{1/2}]$ being the refractive index.[24] In the vicinity of the transparency, $\omega \cdot dn_r/d\omega$ can be significantly larger than n_r in magnitude. Figure 4c shows an intensity plot of the simulated group index, where n_g can be as large as 500, or even negative in a narrow spectral window. To experimentally observe the slow light effect, multiple stacked bilayer graphene might be needed.[13] Alternatively, graphene ribbons on waveguide structures[37] can largely enhance the light-matter interaction and amplify the slow-light effect. The calculated results indicate that bilayer graphene ribbons can potentially have dramatic effect on the propagation and interaction of infrared photons.

Summary. In summary, we have reported a novel phonon-induced transparency (PIT) phenomenon in the plasmonic response of bilayer graphene and demonstrated the wide tunability of this phenomenon, both passively and actively. Our microscopic theoretical model is in good agreement with the experimental observations, accounting for both the plasmonic enhancement of phonon infrared activity and the spectrally sharp transparency. In addition, PIT is usually accompanied by strong distortion in light dispersion, leading to a strong slow light effect. Our study, therefore, opens up a new avenue for EIT-like phenomenon in bilayer graphene metamaterials via its internal lattice vibration mode and paves the way for various applications in few-photon nonlinear optics, quantum optics and slow light devices.

Methods. *Sample Preparation, Fabrication, and Measurement.* Graphene flakes on high resistivity SiO_2/Si substrate were mechanically exfoliated from graphite. The oxide thickness of the substrate is 90 nm. Multilayer graphene flakes obtained in this way preserve good stacking order. Bilayer graphene, which is the focus of this paper, was identified by Raman and confirmed by infrared spectroscopy. Large area (>100 μm in dimension) bilayer graphene flakes were chosen to make graphene nanoribbon arrays with area of 60 × 60 μm using electron beam lithography and oxygen plasma etching. The ribbon width was designed to be the same as or slightly larger than the gap between ribbons. For some of the ribbon arrays, Ti/Au metal contacts were also deposited to enable back gating.

The as-prepared ribbons are usually hole-doped (Fermi level $\mu < 0$). For the ribbons without metal contacts, the doping level can be increased further by exposing the samples to the nitric acid vapor for 10 min. The doping due to nitric acid can be removed partially or completely in ambient condition or by baking. As a consequence, we could achieve different doping levels. For the ribbons with metal contacts, we were able to actively change the Fermi level by a back gate.

The extinction measurements were done in a transmission geometry using a Nicolet 8700 FT-IR in conjunction with an IR-microscope. The IR beam size is ∼25 μm which is smaller than the ribbon array. To minimize the water absorption in the air, nitrogen gas was purged in the FT-IR chamber and the sample area. We measured the transmission T_S through the bare area without graphene on the wafer as a reference and the transmission T through the ribbon array with polarization either parallel or perpendicular to the ribbon axis. The extinction is defined as $1 - T/T_S$.

Tight Binding Model for Bilayer Graphene. In the band structure calculation, we consider a bilayer graphene arranged in the Bernal AB stacking order as depicted in the inset of Figure 1b. Following McCann,[33] we work in the 4 × 4 basis of atomic p_z orbitals $(a_1^\dagger, b_1^\dagger, a_2^\dagger, b_2^\dagger)$ where $a_i^\dagger$and $b_i^\dagger$are creation operators for the i^{th} layer on the sublattice A or B respectively. In this basis, the Hamiltonian near the **K** point can be written as

$$\hat{H}_k = v_f \pi_+ \hat{I} \otimes \hat{\sigma}_- + v_f \pi_- \hat{I} \otimes \hat{\sigma}_+ + (\Delta/2)\hat{\sigma}_z \otimes \hat{I} + (\gamma_1/2)[\hat{\sigma}_x \otimes \hat{\sigma}_x + \hat{\sigma}_y \otimes \hat{\sigma}_y]$$

where $\hat{\sigma}_i$ and $\hat{I}$ are the 2 × 2 Pauli and identity matrices, respectively, and we have defined $\hat{\sigma}_\pm = 1/2\ (\hat{\sigma}_x \pm i\hat{\sigma}_y)$and $\pi_\pm = \hbar(k_x \pm ik_y)$. Here, v_f is the Fermi velocity, γ_1 the interlayer hopping, and Δ is the electrostatic potential difference between the two layers. We derived the noninteracting ground state electronic bands and wave functions by diagonalizing the above Hamiltonian, see Supporting Information for details.

■ ASSOCIATED CONTENT

Supporting Information

Detailed theoretical calculation method, Raman spectrum of bilayer graphene, description of the coupled oscillator model, plasmons in trilayer graphene nanoribbons, Fano parameter analysis. This material is available free of charge via the Internet at http://pubs.acs.org.

dx.doi.org/10.1021/nl501628x | Nano Lett. 2014, 14, 4581−4586

AUTHOR INFORMATION

Corresponding Authors

*E-mail: hyan@us.ibm.com (H. Y.).
*E-mail: tonyaslow@gmail.com (T. L.).
*E-mail: fengnian.xia@yale.edu (F. X.).
*E-mail: avouris@us.ibm.com (P. A.).

Author Contributions

⊥These authors contributed equally to the work.

Notes

The authors declare no competing financial interest.

ACKNOWLEDGMENTS

The authors are grateful to H. Wang, W. Zhu, D. Farmer, M. Freitag, G. Tulevski, Y. Li, B. Ek, and J. Bucchignano for experimental assistance in device fabrication and characterization. T.L. and F.G. acknowledge hospitality of KITP, supported in part by the NSF grant no. NSF PHY11-25915. T.L. also acknowledges partial support from NRI-INDEX and F.G. is also supported by the Spanish MICINN (FIS2008-00124, CONSOLIDER CSD2007-00010) and ERC grant 290846.

REFERENCES

(1) Harris, S. E. *Phys. Today* **1997**, *50*, 36−42.
(2) Xu, Q.; Sandhu, S.; Povinelli, M. L.; Shakya, J.; Fan, S.; Lipson, M. *Phys. Rev. Lett.* **2006**, *96* (12), 123901.
(3) Zhang, S.; Genov, D. A.; Wang, Y.; Liu, M.; Zhang, X. *Phys. Rev. Lett.* **2008**, *101* (4), 047401.
(4) Gu, J.; Singh, R.; Liu, X.; Zhang, X.; Ma, Y.; Zhang, S.; Maier, S. A.; Tian, Z.; Azad, A. K.; Chen, H.-T.; Taylor, A. J.; Han, J.; Zhang, W. *Nature Commun.* **2012**, *3*, 1151.
(5) Liu, N.; Langguth, L.; Weiss, T.; Kastel, J.; Fleischhauer, M.; Pfau, T.; Giessen, H. *Nat. Mater.* **2009**, *8* (9), 758−762.
(6) Kurter, C.; Tassin, P.; Zhang, L.; Koschny, T.; Zhuravel, A. P.; Ustinov, A. V.; Anlage, S. M.; Soukoulis, C. M. *Phys. Rev. Lett.* **2011**, *107* (4), 043901.
(7) Weis, S.; Riviere, R.; Deleglise, S.; Gavartin, E.; Arcizet, O.; Schliesser, A.; Kippenberg, T. J. *Science* **2010**, *330* (6010), 1520−1523.
(8) Xia, F.; Sekaric, L.; Vlasov, Y. *Nat. Photonics* **2007**, *1* (1), 65−71.
(9) Dong, Z.; Hui, L.; Jing-Xiao, C.; Tao, L.; Shu-Ming, W.; Shi-Ning, Z.; Zhang, X. *Appl. Phys. Lett.* **2010**, *97* (11), 114101.
(10) Ju, L.; Geng, B.; Horng, J.; Girit, C.; Martin, M.; Hao, Z.; Bechtel, H. A.; Liang, X.; Zettl, A.; Shen, Y. R.; Wang, F. *Nat. Nanotechnol.* **2011**, *6* (10), 630−634.
(11) Fei, Z.; Rodin, A. S.; Andreev, G. O.; Bao, W.; McLeod, A. S.; Wagner, M.; Zhang, L. M.; Zhao, Z.; Thiemens, M.; Dominguez, G.; Fogler, M. M.; Neto, A. H. C.; Lau, C. N.; Keilmann, F.; Basov, D. N. *Nature* **2012**, *487*, 82−85.
(12) Chen, J.; Badioli, M.; Alonso-Gonzalez, P.; Thongrattanasiri, S.; Huth, F.; Osmond, J.; Spasenovic, M.; Centeno, A.; Pesquera, A.; Godignon, P.; Zurutuza Elorza, A.; Camara, N.; de Abajo, F. J. G.; Hillenbrand, R.; Koppens, F. H. L. *Nature* **2012**, *487*, 77−81.
(13) Yan, H.; Li, X.; Chandra, B.; Tulevski, G.; Wu, Y.; Freitag, M.; Zhu, W.; Avouris, P.; Xia, F. *Nat. Nanotechnol.* **2012**, *7* (5), 330−334.
(14) Yan, H.; Low, T.; Zhu, W.; Wu, Y.; Freitag, M.; Li, X.; Guinea, F.; Avouris, P.; Xia, F. *Nat. Photonics* **2013**, *7* (5), 394−399.
(15) Zhang, Y.; Tang, T.-T.; Girit, C.; Hao, Z.; Martin, M. C.; Zettl, A.; Crommie, M. F.; Shen, Y. R.; Wang, F. *Nature* **2009**, *459* (7248), 820−823.
(16) Tang, T. T.; Zhang, Y.; Park, C.-H.; Geng, B.; Girit, C.; Hao, Z.; Martin, M. C.; Zettl, A.; Crommie, M. F.; Louie, S. G.; Shen, Y. R.; Wang, F. *Nat. Nanotechnol.* **2010**, *5* (1), 32−36.
(17) Kuzmenko, A. B.; Benfatto, L.; Cappelluti, E.; Crassee, I.; van der Marel, D.; Blake, P.; Novoselov, K. S.; Geim, A. K. *Phys. Rev. Lett.* **2009**, *103* (11), 116804.
(18) Fano, U. *Phys. Rev.* **1961**, *124* (6), 1866−1878.
(19) Jiang, Y. W.; Zhu, K. D. *Appl. Phys. B: Laser Opt.* **2008**, *90* (1), 79−85.
(20) Ferrari, A. C.; Meyer, J. C.; Scardaci, V.; Casiraghi, C.; Lazzeri, M.; Mauri, F.; Piscanec, S.; Jiang, D.; Novoselov, K. S.; Roth, S.; Geim, A. K. *Phys. Rev. Lett.* **2006**, *97* (18), 187401.
(21) Rice, M. J. *Phys. Rev. Lett.* **1976**, *37* (1), 36−39.
(22) Cappelluti, E.; Benfatto, L.; Manzardo, M.; Kuzmenko, A. B. *Phys. Rev. B* **2012**, *86* (11), 115439.
(23) Fei, Z.; Andreev, G. O.; Bao, W.; Zhang, L. M.; S. McLeod, A.; Wang, C.; Stewart, M. K.; Zhao, Z.; Dominguez, G.; Thiemens, M.; Fogler, M. M.; Tauber, M. J.; Castro-Neto, A. H.; Lau, C. N.; Keilmann, F.; Basov, D. N. *Nano Lett.* **2011**, *11* (11), 4701−4705.
(24) Hau, L. V.; Harris, S. E.; Dutton, Z.; Behroozi, C. H. *Nature* **1999**, *397* (6720), 594−598.
(25) Tanji-Suzuki, H.; Landig, R.; Simon, J.; Vuletic, V. *Science* **2011**, *333* (6047), 1266−1269.
(26) Garrido Alzar, C. L.; Martinez, M. A. G.; Nussenzveig, P. *Am. J. of Phys.* **2002**, *70* (1), 37−41.
(27) Neubrech, F.; Pucci, A.; Cornelius, T. W.; Karim, S.; Garcia-Etxarri, A.; Aizpurua, J. *Phys. Rev. Lett.* **2008**, *101* (15), 157403.
(28) Li, Z.; Lui, C. H.; Cappelluti, E.; Benfatto, L.; Mak, K. F.; Carr, G. L.; Shan, J.; Heinz, T. F. *Phys. Rev. Lett.* **2012**, *108* (15), 156801.
(29) Li, Y.; Yan, H.; Farmer, D. B.; Meng, X.; Zhu, W.; Osgood, R. M.; Heinz, T. F.; Avouris, P. *Nano Lett.* **2014**, *14* (3), 1573−1577.
(30) Brar, V. W.; Jang, M. S.; Sherrott, M.; Kim, S.; Lopez, J. J.; Kim, L. B.; Choi, M.; Atwater, H. *Nano Lett.* **2014**, *14* (7), 3876−3880.
(31) Li, Z. Q.; Henriksen, E. A.; Jiang, Z.; Hao, Z.; Martin, M. C.; Kim, P.; Stormer, H. L.; Basov, D. N. *Nat. Phys.* **2008**, *4* (7), 532−535.
(32) Yan, H.; Xia, F.; Zhu, W.; Freitag, M.; Dimitrakopoulos, C.; Bol, A. A.; Tulevski, G.; Avouris, P. *ACS Nano* **2011**, *5* (12), 9854−9860.
(33) McCann, E. *Phys. Rev. B: Condens. Matter Mater. Phys.* **2006**, *74* (16), 161403.
(34) Mahan, G. D. *Many-Particle Physics*, 3rd ed.; Kluwer Academic/Plenum: New York, 2000.
(35) Hwang, E. H.; Das Sarma, S. *Phys. Rev. B: Condens. Matter Mater. Phys.* **2007**, *75* (20), 205418.
(36) Wunsch, B.; Stauber, T.; Guinea, F. *New J. Phys.* **2006**, *8*, 318.
(37) Liu, M.; Yin, X.; Ulin-Avila, E.; Geng, B.; Zentgraf, T.; Ju, L.; Wang, F.; Zhang, X. *Nature* **2011**, *474* (7349), 64−67.